Friction Estimation for Torque Control of Electro-Mechanical Flight Surface Actuation

SCHALLERT Christian
German Aerospace Center (DLR e.V.)
Institute of System Dynamics and Control
82234 Wessling, Germany
Phone: +49 (0) 8153 28 2408
Email: christian.schallert@dlr.de

ABSTRACT

Electro-mechanical actuation (EMA) is pursued for primary flight control of future commercial aircraft. This technology is expected to save effort and related cost of manufacture and maintenance.

Primary flight control EMAs will be typically designed to have a high gear ratio between the motor and surface. This involves significant inertia and friction torques that must be handled by the actuator controller. The friction can vary substantially, since the actuators are exposed to changing loads and a wide temperature range.

This paper describes a state observer that estimates an EMA's friction. It is assumed to include a static and a viscous share. The observer is employed for an adaptive concept of surface torque control.

The described concept has been investigated by means of simulation, test rig experiments are being prepared.

KEYWORDS

Electric actuation, friction estimation and compensation, observer, primary flight surfaces, torque control

I INTRODUCTION

Electric and hydraulic actuators are controlled differently. For the latter, the motion rate depends on the servo-valve current. It is thus obvious to regulate the position, which is well established in contemporary flight control systems.

An electric actuator's (electro-mechanical or electro-hydrostatic, EMA or EHA) output torque is nearly proportional to the motor current. Thus, regulating the surface torque appears feasible and attractive, since an aircraft's motion is governed by aerodynamic forces. A flight control system that regulates surface torques can be simpler than the state-of-the-art, because the torque demands around the aircraft axes do not need to be converted into surface position demands. Rather, they can be used directly for signalling the torque-controlled actuation. As a by-product, a dynamic gust load alleviation is achieved (Schallert and Kowalski, 2023).

Aircraft control using surface torques has been successfully demonstrated by the DLR in collaboration with the TU Delft on the PHLAB test aircraft, a modified Cessna Citation 550 (van der Linden et al., 2018), (Pollack et al., 2019). This aircraft has a mechanical, reversible flight control system with negligible friction.

For larger aircraft with irreversible flight control systems, typical high gear ratio EMA designs involve significant friction that can vary substantially, since the actuators carry changing loads and are exposed to a wide temperature range (Maré, 2012), (Maré, 2014). The variation of friction must be considered for an EMA torque controller.

Hence, this paper describes a state observer that estimates an EMA's friction. It is assumed to include a static τ_{stic} and a viscous τ_{visc} share that depend on the speed. The observer is designed to separately recognise the static and viscous friction parameters that change relatively slowly with the temperature. Since the observer shall suit for implementation on an EMA's control unit and needs to be real-time capable, dependency of the friction on load or the Stribeck effect are omitted for simplicity.

The state observer is employed for an adaptive concept of surface torque control (Schallert and Michel, 2023), as depicted in Figure 1. The controller includes a feedforward (FF) and a feedback (FB). The FF is essentially an inverse model of the plant, i.e. the EMA, that computes the motor (M) voltage required to move the flight surface according to the torque demand T_{dmd}. To this end, the feedforward compensates, amongst others, the plant's inertia and friction.

Generally, a state observer is a model of the corresponding plant used to reconstruct non-measurable plant states. As depicted, the observer receives the same input vector u as the plant. By feedback of $K\Delta y = K(y - \hat{y})$, i.e. an amplified difference of the measurements y and observer outputs $\hat{y}$, the observer states $\hat{x}$ track those of the plant. Friction estimation

is performed by two additional observer states $\hat{\tau}_{stic}$ and $\hat{\tau}_{visc}$ that are low-pass filtered to adapt the controller.
Related observer concepts are also known as online parameter estimation; for instance, as described by (Olsson and Astroem, 1996), (Schuette et al., 1997) and (Beckmann et al., 2015). Adhesion estimation is important also in rail transportation, where suitable observers have been developed by (Schwarz et al., 2019) and (Schwarz and Keck, 2019).

minimised. This way, the interior, non-measurable plant states, such as friction, are identified.
For an EMA, the following non-linear, continuous state observer model is established:

$$\ddot{\hat{\varphi}} = -\frac{1}{J_{tot}}\left(\frac{2\hat{\tau}_{stic}}{1+e^{-sR\dot{\hat{\varphi}}}} - \hat{\tau}_{stic}\right) - \frac{R}{J_{tot}}\hat{\tau}_{visc}\dot{\hat{\varphi}} + \frac{k_M}{J_{tot}}I - \frac{1}{J_{tot}R}T \tag{3}$$

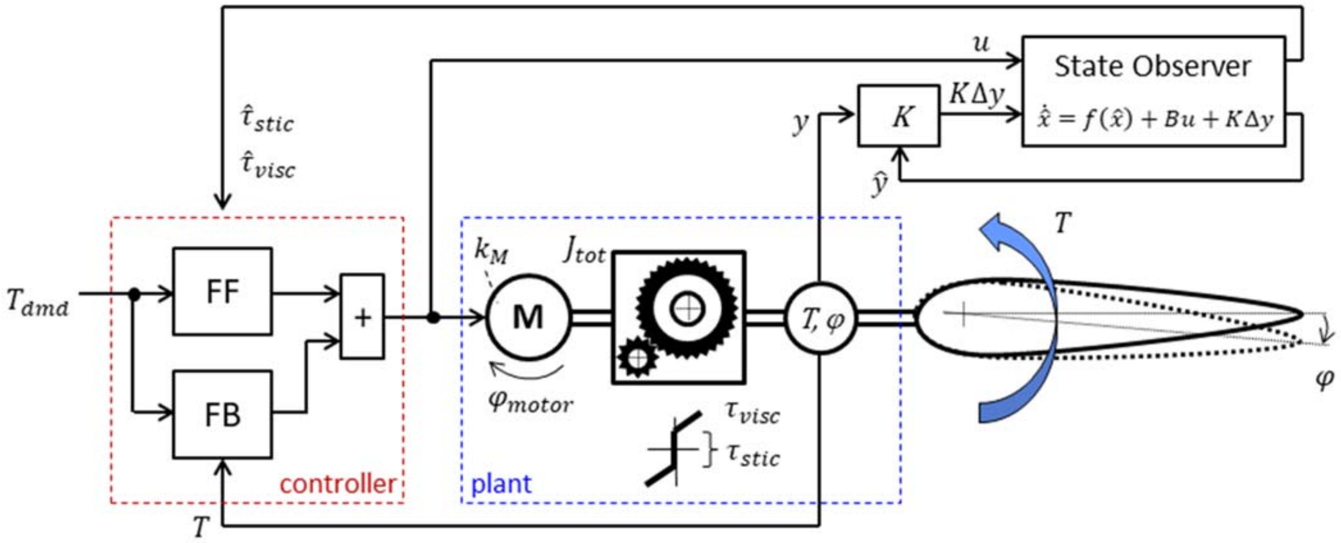

Figure 1. Torque control of electro-mechanical flight surface actuation with a state observer for friction estimation

II FRICTION ESTIMATION

2.1 Friction Model

The observer uses the following non-linear definition of the friction torque T_F dependent on the speed ω (Reiner, 2010):

$$T_F = \frac{2\tau_{stic}}{1+e^{-s\omega}} - \tau_{stic} + \tau_{visc}\omega \tag{1}$$

The stiction and viscous friction are denoted by τ_{stic} and τ_{visc}, respectively, as shown in Figure 2. For invertibility, the stiction is approximated near zero speed with the steepness denoted by s. This invertible, continuous friction model has proven to be suitable for model-based control of industrial robots (Reiner, 2010), and hence it is used as well for the control concept and state observer described in this paper.

2.2 State Observer Model

In its general form, a non-linear state observer is described as

$$\dot{\hat{\boldsymbol{x}}} = f(\hat{\boldsymbol{x}}) + \boldsymbol{B}\boldsymbol{u} + \boldsymbol{K}\Delta\boldsymbol{y}, \tag{2}$$

in which $\hat{\boldsymbol{x}}$ denotes the state vector, $f(\hat{\boldsymbol{x}})$ a non-linear function of the states $\hat{\boldsymbol{x}}$, $\boldsymbol{B}$ the input matrix, $\boldsymbol{K}$ a feedback matrix and $\boldsymbol{y}$ the measurable outputs. Observer quantities are marked with $\widehat{\ }$. By feedback of $\boldsymbol{K}\Delta\boldsymbol{y} = \boldsymbol{K}(\boldsymbol{y} - \hat{\boldsymbol{y}})$, the differences between the observer states $\hat{\boldsymbol{x}}$ and the actual plant states $\boldsymbol{x}$ are

The motor current, actuator output torque and observer input vector are denoted by I, T and $\boldsymbol{u} = \{I,\ T\}^T$, respectively. Furthermore, k_M specifies the motor torque coefficient, J_{tot} the actuator's total coupled inertia, and $R = \varphi_{motor}/\varphi$ the total gear ratio, as indicated in Figure 1. The surface angle, angular velocity and acceleration are denoted by $\hat{\varphi}$, $\dot{\hat{\varphi}}$ and $\ddot{\hat{\varphi}}$, respectively. The estimated stiction and viscous friction are referred to the motor shaft and are denoted by $\hat{\tau}_{stic}$ and $\hat{\tau}_{visc}$. The angular velocity is converted to the motor shaft by $\omega = R\dot{\varphi}$, refer to equation (1). Thus, equation (3) resembles the first two terms of the general form given by equation (2). As regards the third term $\boldsymbol{K}\Delta\boldsymbol{y}$, it is described by equations (10) and (11) how the measurements $y = \{\dot{\varphi},\ \varphi\}^T$ are incorporated in the observer states.
The observer model according to (3) is approximated by a linearised, continuous equation system of the type

$$\dot{\hat{\boldsymbol{x}}} = \frac{\delta f(\hat{\boldsymbol{x}})}{\delta\hat{\boldsymbol{x}}}\hat{\boldsymbol{x}} + \boldsymbol{B}\boldsymbol{u} \tag{4}$$

with $\dot{\hat{\boldsymbol{x}}} = \{\ddot{\hat{\varphi}},\ \dot{\hat{\varphi}},\ 0\}^T$ and the Jacobian matrix $\delta f(\hat{\boldsymbol{x}})/\delta\hat{\boldsymbol{x}}$ that includes all partial derivatives. Since the partial derivatives depend on the states $\hat{\boldsymbol{x}}$, the Jacobian matrix has to be updated continuously in order to achieve accurate computation of equation (4). This is performed in each time step for the discretised observer described by equations (7) through (12).

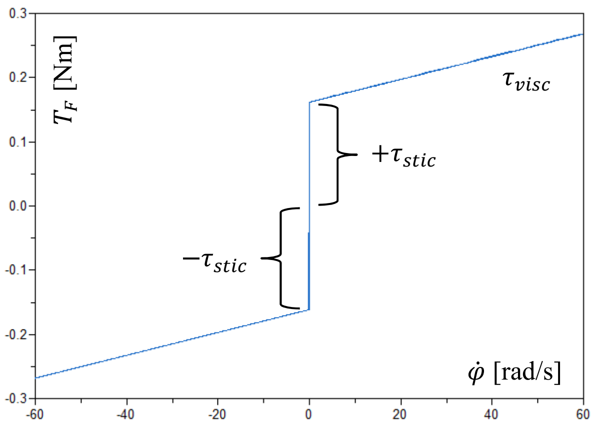

Figure 2. Speed-dependent modelling of stiction and viscous friction

2.3 Discretised Implementation of the Friction Observer

2.3.1 Observer Structure

A cascaded structure has been selected for implementation of the discrete friction observer, with a partial observer both for the stiction and the viscous friction. They use the state vectors $\hat{\boldsymbol{x}}_S = \{\hat{\dot{\varphi}},\, \hat{\varphi},\, \hat{\tau}_{stic}\}^T$ and $\hat{\boldsymbol{x}}_V = \{\hat{\dot{\varphi}},\, \hat{\varphi},\, \hat{\tau}_{visc}\}^T$, respectively. Both partial observers receive the same input $\boldsymbol{u}$ and measurement signals $\boldsymbol{y}$. As depicted in Figure 3, the partial observers are interconnected to exchange the estimated stiction and viscous friction.
The stiction can be identified and hence the output $\hat{\tau}_{stic}$ be updated only if the angular velocity $\dot{\varphi}$ is close to zero. If this is not the case, $\hat{\tau}_{stic}$ remains constant at the last estimated value. Accordingly, a threshold of $\pm\dot{\varphi}_{thresh} = \pm 0.05$ rad/s has been defined; i.e. the stiction observer updates if $-\dot{\varphi}_{thresh} \leq \dot{\varphi} \leq +\dot{\varphi}_{thresh}$.
The viscous friction can be estimated and the output $\hat{\tau}_{visc}$ be updated only at larger angular velocities. If the angular velocity is nearly zero, the output $\hat{\tau}_{visc}$ is kept constant at the last estimated value.

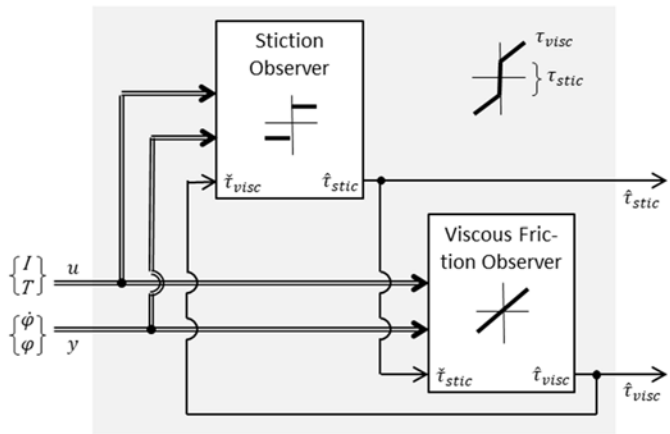

Figure 3. Cascaded structure of the friction observer

The friction observer's behaviour is explained in more detail in subsection 2.4 that shows simulation results.
Eventually, the estimated stiction $\hat{\tau}_{stic}$ and viscous friction $\hat{\tau}_{visc}$ are used to adapt the EMA torque controller, as shown in Figure 1.
In the following, the partial observers for static and viscous friction are described in detail.

2.3.2 Partial Observer for Static Friction

To estimate the static friction, $\hat{\tau}_{stic}$ needs to be introduced as an additional third state, i.e. $\hat{x}_{S,3} = \hat{\tau}_{stic}$, as described. Since no dynamics can be formulated for the change of the stiction, it is set that $\dot{\hat{x}}_{S,3} = \dot{\hat{\tau}}_{stic} = 0$. In addition, the viscous friction, marked here as $\check{\tau}_{visc}$ (see Figure 3), is assumed to be known. For a linearised third order system of equations, refer to equation (4), the Jacobian matrix is generally defined as

$$\frac{\delta f(\hat{\boldsymbol{x}})}{\delta \hat{\boldsymbol{x}}} = \begin{bmatrix} \frac{\delta f_1(\hat{\boldsymbol{x}})}{\delta \hat{x}_1} & \frac{\delta f_1(\hat{\boldsymbol{x}})}{\delta \hat{x}_2} & \frac{\delta f_1(\hat{\boldsymbol{x}})}{\delta \hat{x}_3} \\ \frac{\delta f_2(\hat{\boldsymbol{x}})}{\delta \hat{x}_1} & \frac{\delta f_2(\hat{\boldsymbol{x}})}{\delta \hat{x}_2} & \frac{\delta f_2(\hat{\boldsymbol{x}})}{\delta \hat{x}_3} \\ \frac{\delta f_3(\hat{\boldsymbol{x}})}{\delta \hat{x}_1} & \frac{\delta f_3(\hat{\boldsymbol{x}})}{\delta \hat{x}_2} & \frac{\delta f_3(\hat{\boldsymbol{x}})}{\delta \hat{x}_3} \end{bmatrix} \tag{5}$$

For the stiction observer, the partial derivatives $\delta f_i(\hat{\boldsymbol{x}})/\delta \hat{\boldsymbol{x}}_j$ are determined from equation (3) as follows:

$$\frac{\delta f_1(\hat{x}_S)}{\delta \hat{x}_{S,1}} = \frac{\delta f_1(\hat{x}_S)}{\delta \hat{\dot{\varphi}}} = -\frac{2\hat{\tau}_{stic} \cdot s \cdot R \cdot e^{-sR\hat{\dot{\varphi}}}}{J_{tot}\left(1+e^{-sR\hat{\dot{\varphi}}}\right)^2} - \frac{R}{J_{tot}} \check{\tau}_{visc}, \tag{6}$$

$$\frac{\delta f_1(\hat{x}_S)}{\delta \hat{x}_{S,2}} = \frac{\delta f_1(\hat{x}_S)}{\delta \hat{\varphi}} = 0, \quad \frac{\delta f_1(\hat{x}_S)}{\delta \hat{x}_{S,3}} = \frac{\delta f_1(\hat{x}_S)}{\delta \hat{\tau}_{stic}} = \frac{1}{J_{tot}}\left(1 - \frac{2}{1+e^{-sR\hat{\dot{\varphi}}}}\right),$$

$$\frac{\delta f_2(\hat{x}_S)}{\delta \hat{x}_{S,1}} = \frac{\delta f_2(\hat{x}_S)}{\delta \hat{\dot{\varphi}}} = 1, \quad \frac{\delta f_2(\hat{x}_S)}{\delta \hat{x}_{S,2}} = 0, \quad \frac{\delta f_2(\hat{x}_S)}{\delta \hat{x}_{S,3}} = 0,$$

$$\frac{\delta f_3(\hat{x}_S)}{\delta \hat{x}_{S,1}} = \frac{\delta f_3(\hat{x}_S)}{\delta \hat{x}_{S,2}} = \frac{\delta f_3(\hat{x}_S)}{\delta \hat{x}_{S,3}} = 0.$$

Based on these partial derivatives, the linearised equation system according to (4) is discretised and implemented as a so-called Extended Kalman-Filter (EKF). An EKF consists of equations (7) through (12) that are evaluated at each sample instant T_s. First, the actual states $\hat{\boldsymbol{x}}_k^-$ are estimated from the previous states $\hat{\boldsymbol{x}}_{k-1}^-$ and inputs $\boldsymbol{u}_{k-1}$ in each time step k for $k = 1, 2, \ldots$:

$$\hat{\boldsymbol{x}}_k^- = \boldsymbol{A}_{k-1}\hat{\boldsymbol{x}}_{k-1} + \boldsymbol{B}_{k-1}\boldsymbol{u}_{k-1} \tag{7}$$

In doing so, the estimation error variance is computed by

$$\boldsymbol{P}_k^- = \boldsymbol{A}_{k-1}\boldsymbol{P}_{k-1}\boldsymbol{A}_{k-1}^T + \boldsymbol{Q} \tag{8}$$

The discrete system and input matrices $\boldsymbol{A}_{k-1}$ and $\boldsymbol{B}_{k-1}$ in equations (7) and (8) are computed using equation (4) and the Jacobian matrix (5) as follows:

$$\boldsymbol{A}_{k-1} = \boldsymbol{e}^{\left(\left[\frac{\delta f}{\delta x}\right]_{\hat{x}_{k-1}} \cdot T_s\right)}, \quad \boldsymbol{B}_{k-1} = \int_0^{T_s} \boldsymbol{e}^{\left(\left[\frac{\delta f}{\delta x}\right]_{\hat{x}_{k-1}} \cdot t\right)} \cdot \boldsymbol{B} \cdot dt \tag{9}$$

In order to correct the estimated states $\hat{\boldsymbol{x}}_k^-$ calculated by (7), measurements are incorporated in a next step. These are the angular velocity and angle at the actuator output, thus $\boldsymbol{y}_k = \{\dot{\varphi}_k,\, \varphi_k\}^T$. To this end, the so-called Kalman-matrix

$$\boldsymbol{K}_k = \boldsymbol{P}_k^- \boldsymbol{H}_k^T (\boldsymbol{H}_k \boldsymbol{P}_k^- \boldsymbol{H}_k^T + \boldsymbol{R})^{-1} \tag{10}$$

is computed, and then $\boldsymbol{K}_k$ is used to calculate the actual states $\hat{\boldsymbol{x}}_k$ and estimation error variance $\boldsymbol{P}_k$ as follows:

$$\hat{\boldsymbol{x}}_k = \hat{\boldsymbol{x}}_k^- + \boldsymbol{K}_k (\boldsymbol{y}_k - \boldsymbol{H}\hat{\boldsymbol{x}}_k^-) \tag{11}$$

$$\boldsymbol{P}_k = (\boldsymbol{I} - \boldsymbol{K}_k \boldsymbol{H}) \boldsymbol{P}_k^- \tag{12}$$

The so-called measurement matrix $\boldsymbol{H}$ is defined as $\boldsymbol{H} = \begin{bmatrix} 1 & 0 & 0 \\ 0 & 1 & 0 \end{bmatrix}$, since the stiction observer has three states and evaluates two measured variables. The matrices $\boldsymbol{Q}$ and $\boldsymbol{R}$ in equations (8) and (10) are covariances that have to be selected according to the expected model and measurement error, respectively. Hence, $\boldsymbol{Q}$ and $\boldsymbol{R}$ are tuning parameters of the Kalman-Filter. For instance, a smaller value for $\boldsymbol{Q}$ and a larger value for $\boldsymbol{R}$ are meaningful, if the observer model is deemed to be of high precision and if the measurements are not trusted as much, e.g. due to signal noise. Then, past observer states are weighted more and actual measurements are weighted less in the computation of the present observer states. For further reference about the Kalman-Filter, the reader is referred to (Welch and Bishop, 2006).

2.3.3 Partial Observer for Viscous Friction

For the viscous friction observer with the state vector $\hat{\boldsymbol{x}}_V = \{\dot{\hat{\varphi}},\ \hat{\varphi},\ \hat{\tau}_{visc}\}^T$, it is set accordingly that $\dot{\hat{x}}_{V,3} = \dot{\hat{\tau}}_{visc} = 0$. In addition, the stiction is assumed to be known as the input signal $\check{\tau}_{stic}$, as indicated in Figure 3. From the observer model of equation (3), the partial derivatives are deduced as follows according to equations (4) and (5):

$$\frac{\delta f_1(\hat{x}_V)}{\delta \hat{x}_{V,1}} = \frac{\delta f_1(\hat{x}_V)}{\delta \dot{\hat{\varphi}}} = -\frac{2\check{\tau}_{stic} \cdot s \cdot R \cdot e^{-sR\dot{\hat{\varphi}}}}{J_{tot}\left(1+e^{-sR\dot{\hat{\varphi}}}\right)^2} - \frac{R}{J_{tot}} \hat{\tau}_{visc}, \tag{13}$$

$$\frac{\delta f_1(\hat{x}_V)}{\delta \hat{x}_{V,2}} = \frac{\delta f_1(\hat{x}_V)}{\delta \hat{\varphi}} = 0, \quad \frac{\delta f_1(\hat{x}_V)}{\delta \hat{x}_{V,3}} = \frac{\delta f_1(\hat{x}_V)}{\delta \hat{\tau}_{visc}} = -\frac{R}{J_{tot}} \dot{\hat{\varphi}}$$

$$\frac{\delta f_2(\hat{x}_V)}{\delta \hat{x}_{V,1}} = \frac{\delta f_2(\hat{x}_V)}{\delta \dot{\hat{\varphi}}} = 1, \quad \frac{\delta f_2(\hat{x}_V)}{\delta \hat{x}_{V,2}} = 0, \quad \frac{\delta f_2(\hat{x}_V)}{\delta \hat{x}_{V,3}} = 0,$$

$$\frac{\delta f_3(\hat{x}_V)}{\delta \hat{x}_{V,1}} = \frac{\delta f_3(\hat{x}_V)}{\delta \hat{x}_{V,2}} = \frac{\delta f_3(\hat{x}_V)}{\delta \hat{x}_{V,3}} = 0.$$

Then, the linearised equation system is implemented as well according to eq. (7) through (12) as a discrete EKF.

2.4 Simulation of Discretised Friction Observer

In order to verify the described entire discretised friction observer (see Figure 3), it has been employed to estimate the static and viscous friction in a simulation environment. In this manner, the observer's estimation capability has been verified for different commands and friction parameters of the EMA. For illustration, Figure 4 shows the simulation result for a sinusodial surface position command with an amplitude of 0.1 rad and a period of 2 s.

In order to simulate realistic conditions, noise has been added to the measurement signals φ, $\dot{\varphi}$ and T according to Table 1. More specifically, noise amplitudes of 0.5 % of the respective measurement ranges have been assumed.

Table 1. Measurement noise

signal		measurement range	noise amplitude
angle	φ	±0.5 rad	±0.0025 rad
angular velocity	$\dot{\varphi}$	±0.7 rad/s	±0.0035 rad/s
torque	T	±400 Nm	±2 Nm

The upper diagrams of Figure 4 (a) and (b) show the noisy measurement of the angular velocity and the thresholds $+\dot{\varphi}_{thresh}$ and $-\dot{\varphi}_{thresh}$ associated with the stiction estimation. (For a better resolution, Figure 4 (b) shows the same simulation result as Figure 4 (a), but with the time axis zoomed in to 8 s to 10 s.) When $|\dot{\varphi}|$ is low, then state $\hat{x}_{S,3}$ and output $\hat{\tau}_{stic}$ of the stiction observer are being updated. Otherwise, when $\dot{\varphi} < -\dot{\varphi}_{thresh}$ or $+\dot{\varphi}_{thresh} < \dot{\varphi}$, then state $\hat{x}_{S,3}$ and output $\hat{\tau}_{stic}$ remain at their last respective values.

The middle diagrams of Figure 4 indicate the reference value set for the EMA stiction τ_{stic}, the observer state $\hat{x}_{S,3}$, and the output $\hat{\tau}_{stic}$ i.e. the estimated stiction. Obviously, due to noise, state $\hat{x}_{S,3}$ can differ significantly from the reference value τ_{stic}. (τ_{stic} and τ_{visc}, as indicated in Figure 4, relate to the reduction gear's input side.) Thus, another filtering was implemented for the output $\hat{\tau}_{stic}$ that incorporates the computed state values $\hat{x}_{S,3}$ in $\hat{\tau}_{stic}$ only when $|\dot{\varphi}|$ is low. This noise attenuation unavoidably introduces a time delay. However, as can be seen in the middle diagrams of Figure 4, after the observer state $\hat{x}_{S,3}$ and output $\hat{\tau}_{stic}$ had been initialised to zero at the start, output $\hat{\tau}_{stic}$ renders the actual stiction τ_{stic} with good accuracy (refer to subsection 2.4.1) after three to four strokes of the actuator.

The viscous friction estimation is indicated by the lower diagrams of Figure 4. As can be seen, the respective state $\hat{x}_{V,3}$ approximates the reference value of the viscous friction τ_{visc} only if the angular velocity is large, i.e. if $|\dot{\hat{\varphi}}| \gg 0$. On that condition, the computed values of the state $\hat{x}_{V,3}$ are incorporated in the filtered output value $\hat{\tau}_{visc}$.

In the time span from approximately 2.5 s to 5 s, the viscous friction $\hat{\tau}_{visc}$ is estimated clearly to high, as can be seen in the lower part of Figure 4. The too high estimation of $\hat{\tau}_{visc}$ can be explained by the stiction $\hat{\tau}_{stic}$ that is estimated too low until approximately 5 s. The partial observer for viscous friction depends on the estimated stiction, indicated as input $\check{\tau}_{stic}$ in Figure 3, and uses the input signals $\boldsymbol{u} = \{I,\ T\}^T$, i.e. the motor current and actuator output torque, to compute at first the entire friction, as can be seen in equation (3). Thus, since the stiction is estimated too low initially, correspondingly the viscous friction is estimated too high. This effect occurs because all observer states and outputs had been initialised to zero. Hence, it takes a few small strokes of the actuator for the observer outputs $\hat{\tau}_{stic}$ and $\hat{\tau}_{visc}$ to render the actual friction of the plant. In addition, the convergent behaviour shows that the entire friction observer is stable.

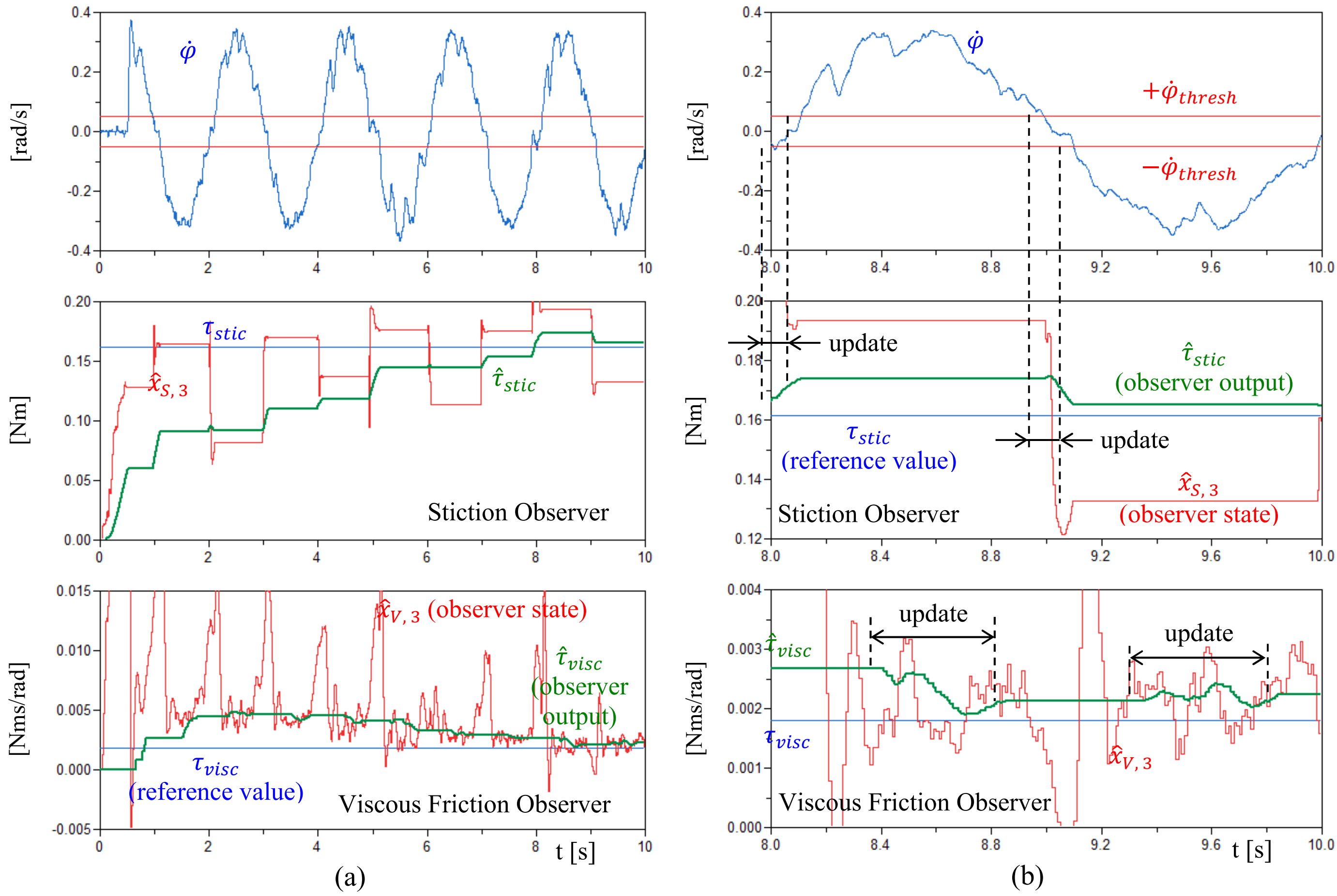

Figure 4. Estimation of static and viscous friction during a sinusodial surface excursion of ±0.1 rad and T = 2 s

Sample times T_s of 0.01 s (viscous friction) and, respectively, 0.005 s (stiction) were selected for the partial observers. Since the stiction can be estimated only when the angular velocity is close to zero and since this occurs for a few tenths of a second when the actuator moves, the shorter sample time i.e. higher resolution improves the estimation accuracy.

2.4.1 Estimation Accuracy

The estimation accuracy of the observer has been examined for different values of static and viscous friction. All combinations of $\tau_{stic} \in \{0;\ 0.08;\ 0.16;\ 0.25\}$ Nm and $\tau_{visc} \in \{5 \cdot 10^{-5};\ 1 \cdot 10^{-4};\ 1 \cdot 10^{-3};\ 5 \cdot 10^{-3};\ 0.01;\ 0.05\}$ Nms/rad, i.e. 24 pairs of values were regarded. Actuator excursions that cause angular velocities of $\max(|\dot{\varphi}|) \in \{0.1;\ 0.2;\ 0.3;\ 0.5;\ 0.7\}$ rad/s were simulated for each pair of τ_{stic} and τ_{visc}, which led to 120 different combinations in total. For each combination, convergence of the estimation was reached within 20 s, and it was found that

- the stiction estimation error is ≤ 0.03 Nm for $\tau_{visc} \leq 0.01$ Nms/rad and ≤ 0.14 Nm for $\tau_{visc} \leq 0.05$ Nms/rad,
- the viscous friction cannot be estimated reliably for angular velocities $|\dot{\varphi}| < 0.3$ rad/s,
- for angular velocities $0.3 \leq |\dot{\varphi}| \leq 0.7$ rad/s, the estimation error is < 10 % of the actual viscous friction.

Thus, the stiction is estimated precisely, if the actuator moves slowly and if the viscous friction does not become too large, i.e. if it is ≤ 0.01 Nms/rad. Otherwise, the observer's ability to distinguish between stiction and viscous friction is diminished. The viscous friction can be estimated more precisely, the higher the angular velocity is.

CONCLUSION

An observer has been developed that estimates an EMA's friction. This observer complements to a flight surface torque controller that has to be adapted when the friction changes, e.g. due to temperature influence. The observer is formulated using the definitions of a so-called Extended Kalman-Filter (EKF) and has been discretised for implementation on a real-time system. A cascaded structure has been selected in order for the observer to estimate the stiction and viscous friction separately. Sensor noise has been considered in order to simulate realistic conditions, and the EKF's filter parameters have been selected appropriately. The observer's capability of estimating the stiction and viscous friction, as well as the estimation accuracy have been verified by numerous simulations that examined different motion and friction parameters of an EMA. Test rig experiments of the described controller and friction observer concept are being prepared.

REFERENCES

Beckmann D., Wielitzka M., Dagen M. and Ortmaier T. (2015), *Online parameter estimation with sensitivity-based excitation monitoring of a mechatronic drive system*, VDI-Berichte Nr. 2268, pp 53-63, Düsseldorf, Germany, 2015.

Maré J.-C. (2012), *Friction modelling and simulation at system level: a practical view for the designer*, Journal of Systems and Control Engineering, 226(6), pp 728-741, January 26, 2012, DOI: 10.1177/0959651812441749

Maré J.-C. (2014), *Friction modelling and simulation at system level: Consideration to load and temperature effects*, Journal of Systems and Control Engineering, pp 1-22, Sept. 28, 2014, DOI: 10.1177/0959651814548440

Olsson H. and Astroem K. J. (1996), *Observer-Based Friction Compensation*, Proceedings of the 35th Conference on Decision and Control, pp 4345-4350, Kobe, Japan, December 1996.

Pollack T., Looye G. and van der Linden F. (2019), *Design and flight testing of flight control laws integrating incremental nonlinear dynamic inversion and servo current control*, AIAA SciTech 2019 Forum, San Diego, CA, USA, Jan. 7-11, 2019, DOI: 10.2514/6.2019-0130

Reiner M. J. (2010), *Modellierung und Steuerung von strukturelastischen Robotern*, Dissertation, Technische Universität München, Germany, 2010.

Schallert C. and Kowalski R. (2023), *LuFo V-3 LLARA Schlussbericht*, TIB Leibniz Information Centre for Science and Technology, University Library, www.tib.eu/en, Hannover, Germany, 21.06.2023.

Schallert C. and Michel K. (2023), *Optimisation of a torque controller for electro-mechanical flight surface actuation*, Proceedings of the R3ASC23 Recent Advances in Aerospace Actuation Systems and Components Conference, Toulouse, France, September 25-27, 2023.

Schallert C. and Michel K. (2023), *Torque controller optimization and robustness analysis for electro-mechanical primary flight surface actuation*, to appear in: AIAA Journal of Guidance, Control, and Dynamics, https://arc.aiaa.org/journal/jgcd.

Schuette F., Beineke S., Rolfsmeier A. and Grotstollen H. (1997), *Online Identification of Mechanical Parameters using Extended Kalman Filters*, Proceedings of the IEEE Industry Applications Society Annual Meeting, pp 501-508, New Orleans, Louisiana, USA, October 5-9, 1997.

Schwarz C., Brembeck J. and Heckmann B. (2019), *Dynamics observer for the longitudinal behavior of a wheelset on a roller rig*, Proceedings of the Institution of Mechanical Engineers, Part F: Journal of Rail and Rapid Transit, Vol. 233(10) pp 1112-1119, February 12, 2019, DOI: 10.1177/0954409719828851

Schwarz C. and Keck A. (2019), *Observer Synthesis for the Adhesion Estimation of a Railway Running Gear*, in IFAC Proceedings Volumes (IFAC-PapersOnline), pp 844-849, Joint Conference 8th IFAC Symposium on Mechatronic Systems and 11th IFAC Symposium on Nonlinear Control Systems, Vienna, Austria, September 4-6, 2019.

Van der Linden F., Looye G. and Pollack T. (2018), *Aircraft Control using Actuator Current*, Proceedings of the R3ASC18 Recent Advances in Aerospace Actuation Systems and Components Conference, pp 196-202, Toulouse, France, May 30 - June 1, 2018.

Welch G. and Bishop G. (2006), *An Introduction to the Kalman-Filter*, TR 95-041, Department of Computer Science, University of North Carolina, Chapel Hill, NC, USA, 27599-3175, 2006.

NOTATIONS

Symbols

$\boldsymbol{A}$	system matrix
$\boldsymbol{B}$	input matrix
e^x	exponential function
$\boldsymbol{H}$	measurement matrix
$\boldsymbol{I}$	identity matrix
J	inertia (kg.m^2)
k_M	motor torque coefficient (Nm/A)
$\boldsymbol{K}$	Kalman matrix
$\boldsymbol{P}$	estimation error variance matrix
$\boldsymbol{Q}$	process (or model) noise covariance matrix
$\boldsymbol{R}$	measurement noise covariance matrix
R	gear ratio (-)
s	steepness of static friction approximation near zero speed
t	time (s)
T	torque (Nm)
T_S	sample time (s)
$\boldsymbol{u}$	input vector
$x, \boldsymbol{x}$	state, state vector
$y, \boldsymbol{y}$	output, output vector
τ_{stic}	stiction (Nm)
τ_{visc}	viscous friction (Nm.s/rad)
ω	angular velocity (rad/s)
$\varphi, \dot{\varphi}, \ddot{\varphi}$	angle (rad), angular velocity (rad/s), and acceleration (rad/s^2)

Subscripts

dmd	demand
F	friction
k, i, j	indices
$thresh$	threshold
tot	total

Superscripts

$\frown$, $\smile$	observer quantities
T	transpose

AKNOWLEDGEMENT

This research has received funding from the German Federal Ministry for Economic Affairs and Climate Action in the frame of the *LuFo V-3 LLARA* joint research project (FKZ: 20Y1706B) that was conducted from 2018 to 2022.